Numerical Prediction of Accumulated Ice Loads on the Fishing Vessel *F.V. Destination* Lost in the Bering Sea

S.R. Dehghani, Y.S. Muzychka, B. Colbourne
Faculty of Engineering and Applied Science, Memorial University of Newfoundland, St. John's

Abstract

This study uses the current knowledge of marine icing to estimate the amount of spray ice load accumulated on the fishing vessel F.V. Destination that sank in the Bering Sea in February 2017. The analysis includes wave-impact sea spray and brine-spongy ice models. The input data including sea conditions, vessel information and weather information are provided by the US NTSB. The main assumptions in the analysis concern the frequency of spray generation, icing surfaces and sufficient water delivery for icing. The results of the icing model are strongly dependent on the input data provided by the NTSB. Results show that the highest rate of ice accumulation is about 2.7 ton/15min which occurred around 1700 AKST on February 10. The overall amount of ice accumulated on the vessel, which is calculated using the upper limits of the assumptions, is about 154 ton. Using the lower limits of the assumptions, this reduces to 92 ton. An analysis was conducted to estimate the effect of the predicted ice accumulation on the vessel stability with the result that the upper ranges of the predicted icing create a high probability of capsizing due to loss of stability

Keywords: Marine icing; FV Destination; Ice accumulation; Numerical model; Capsizing

Nomenclature

c_a	Specific heat capacity of air $(J/kg.K)$
c_b	Specific heat capacity of brine $(J/kg.K)$
c_e	Equivalent specific heat capacity of brine-spongy ice $(J/kg.K)$
c_i	Specific heat capacity of ice $(J/kg.K)$
c_s	Specific heat capacity of brine-spongy ice $(J/kg.K)$
e_s	Standard vapor pressure over the brine surface (Pa)
H_s	Significant wave height (m)
h	Convection heat transfer coefficient $(W/m^2.K)$
i	Node number (---)
k_a	Thermal conductivity of air $(W/m.K)$
k_b	Thermal conductivity of brine $(W/m.K)$
k_i	Thermal conductivity of ice $(W/m.K)$
k_s	Thermal conductivity of brine-spongy ice $(W/m.K)$
L	Length scale (m)
L_{Hb}	Latent heat of fusion of brine (J/kg)

L_{Hv} Latent heat of vaporization of brine (J/kg)
m Number of the node of solid phase closest to the phase interface (---)
Nu Nusselt number (---)
n Number of the discretized grids (---)
P Wave period (s)
P_a Atmospheric pressure (Pa)
Pr Prandtl number (---)
Q_e Evaporation heat flux (J/s)
Q_h Convection heat flux (J/s)
Q_r Radiant heat flux (J/s)
Re Reynolds number (---)
RH Relative humidity (%)
S Overall salinity (‰)
S_b Salinity of brine pockets (‰)
Sc Schmidt number (---)
T Temperature (^{o}C)
T_a Ambient temperature (^{o}C)
T_b Temperature of brine layer (^{o}C)
T_{b1} First interpolated temperature of liquid phase (^{o}C)
T_{b2} Second interpolated temperature of liquid phase (^{o}C)
T_f Freezing temperature of brine (^{o}C)
T_i Initial temperature (^{o}C)
T_{s1} First interpolated temperature of solid phase (^{o}C)
T_{s2} Second interpolated temperature of solid phase (^{o}C)
t Time (s)
t_0 Initial time (s)
U_r Relative velocity (m/s)
V_{Fb} Volume fraction of brine (---)
V_a Wind speed (m/s)
V_s Vessel speed (m/s)
X Phase interface position (m)
X_e The extent of the spray cloud (m)
α_{cb} Coefficient of the equation of specific heat capacity of brine (---)
α_{ci} Coefficient of the equation of specific heat capacity of ice (---)
α_{kb} Coefficient of the equation of thermal conductivity of brine (---)
α_{ki} Coefficient of the equation of thermal conductivity of ice (---)
α_{LHb} Coefficient of the equation of latent heat of fusion of brine (---)
α_{sb} Coefficient of the equation of salinity of brine (---)
$\alpha_{\rho b}$ Coefficient of the equation of density of brine (---)

$\alpha_{\rho i}$ Coefficient of the equation of density of ice (---)
ε Ratio of molecular weight of water and dry air (---)
ε_a Emissivity of air flow (---)
ε_b Emissivity of brine surface (---)
μ_a Viscosity of air ($kg/m.s$)
ρ_a Density of air (kg/m^3)
ρ_b Density of brine (kg/m^3)
ρ_e Equivalent density of brine-spongy ice (kg/m^3)
ρ_i Density of ice (kg/m^3)
ρ_s Density of brine-spongy ice (kg/m^3)
δ Freezing fraction of solidification (---)
σ Stefan-Boltzmann constant ($W/m^2.K^4$)

1. Introduction

Marine icing poses considerable safety issues such as risks to the stability of marine vessels and to the safety of the crew during harsh weather conditions. There are many reports on fishing vessel sinkings due to marine icing. Hay (1956) reported the loss of the trawlers "Lorella" and "Roderigo" as a result of sea spray icing in the fishing grounds north of Iceland in January 1955. Blackmore and Lozowski (1994) reported that this accident was actually the beginning of research on the ship icing problems. Shekhtman (1971) reported that 10 Soviet ships in the Bering Sea were lost due to instability by the formation of ice in January 1965. Zakrzewski and Lozowski (1988) reported that many vessel losses have occurred due to icing. In the 1980s, Jørgensen (1982) reported the risks of superstructure icing due to seawater spray and atmospheric icing because of precipitation on offshore platforms. Ryerson (2011) covered the hazards of icing, which include: instability and loss of integrity of ships and offshore structures, malfunction of the operational equipment and communication antennas, slippery handrails, ladders or decks, unusable lifeboats and fire equipment, and the blocking of air vents.

The icing phenomenon on marine vessels in the Arctic and other cold regions: atmospheric icing and marine or sea spray icing (Aksyutin, 1979; Shekhtman, 1971). Sea spray icing, or marine icing, occurs for two distinct reasons: wave-generated spray and wind-generated spray. Wave spray arises from the impingement of waves on marine vessels and structures. Wave-generated spray is generally a significant source that is a short and approximately periodic water flux created near the bow of vessels and the base of offshore structures. Wind-generated spray is a smaller source, but is a constant water flux that is created in the airflow during windy conditions. According to previous studies (Zakrzewski, 1986), sea spray is the main reason for icing in cold regions. Some parameters have considerable impacts on the icing phenomenon and ice accretion during a sea spray event. These include: (1) environmental factors such as wind velocity, air temperature, droplets temperature, the freezing temperature of seawater, salinity, the size and distribution of droplets, relative humidity, characteristics of swell waves (height, period,

propagation direction), sea or ocean conditions, and (2) the characteristics of marine vessels, including size and design of the vessels, vessel speed, and the angle between the vessel heading and wind/wave direction (Bodaghkhani et al., 2016; Dehghani-Sanij et al., 2017; Dehghani et al., 2016a, 2016b).

Ice accretion models for marine icing phenomena require the rate of droplets traveling over a marine vessel and hitting freezing surfaces. Velocities and sizes determine the rate of heat transfer, vaporization and temperature changes of droplets. Droplet temperatures at the moment of impingement on the freezing surface add internal energy to the energy balance for the brine layer. In the case of frozen droplets, they add latent heat of fusion to the energy balance equation. The rate of mass flux of water to the freezing surface is determined based on droplet sizes and velocities (Dehghani et al., 2018; Dehghani et al., 2016b).

The freezing of a thin layer of salt water and estimating the rate of ice accretion on cold substrates are challenging phenomena. Intermittent ice accretion due to wave-impact sea spray is a dominant mechanism of ice accretion that depends on heat transfer through the spongy substrate. The brine layer starts freezing by releasing and dissipating the latent heat of fusion through the substrate. The resultant ice is a two-phase medium including pure ice and trapped brine pockets. This type of freezing involves a two-phase substrate called spongy ice and a thin layer of a solution of water and salt called the brine layer. Trapped brine pockets, existing between pure ice dendrites, fill the porosity of the ice medium and create spongy ice (Dehghani et al., 2018; Schiesser and Griffiths, 2009).

Accumulation of the first layer of spongy ice on a substrate of spongy ice affects the rate of ice accretion for the next layers. Estimating the thickness of spongy ice accumulated on marine structures has been an important subject of research for many years. The method of the control volume, which considers the average of the properties in target systems and is not an accurate method for fast phenomena with high gradients of properties, has been the main method of approach. A cold substrate of spongy ice is capable of absorbing the released latent heat of fusion that can control the rate of ice accretion. A substrate of spongy ice acts as a thermal capacitor in the process of ice accretion. In the cooling process, spongy ice becomes colder and the trapped brine pockets start to freeze and join the pure ice. The amount of freezing of the brine pockets depends on the corresponding cooling process and the final temperature of the spongy ice (Dehghani et al., 2017; Dehghani et al., 2018).

The ice accumulated on the subject fishing vessel is calculated numerically using environmental and vessel data provided by NTSB. The numerical scheme uses the current published knowledge of marine icing phenomena and a numerical code which is recently developed by the authors. The results are strongly dependent on the input data and despite having considerable information related to this case, there are some unknown parameters that can cause uncertainties.

2. Wave-spray ice accretion

The impact of a wave on a vessel bow creates a thin and unstable sheet of water on the bow surface (Dehghani et al., 2016a). The sheet of water splits into several strips. As the strips become unstable, they are divided into many droplets. The result is a cloud of spray which is called a wave-impact sea spray (Dehghani et al., 2016a). Wave-impact sea spray includes droplets of various sizes and velocities. The droplets travel over the marine vessel or the offshore structure to impinge on a surface or pass over the platform and return to the sea (Lozowski et al., 2000; Zakrzewski, 1987). The spray duration is a short period in the intervals of the wave impact. The wave-impact sea spray is an intermittent phenomenon and strongly dependent on time (Kulyakhtin and Tsarau, 2014; Ryerson, 1995). Fig. 1 illustrates wave-impact sea spray on a vessel bow.

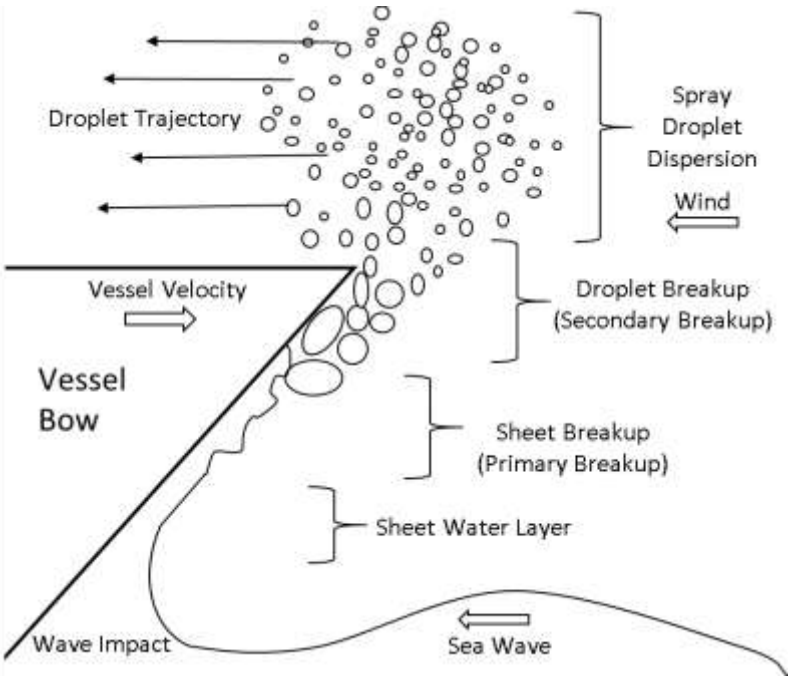

Fig. 1. Wave-impact sea spray on a vessel bow (Dehghani et al., 2016a).

The incoming water on the front edge of marine vessels and offshore structures can be estimated based on the Liquid Water Content (LWC) and water flux (Forest et al., 2005; Zakrzewski, 1987). The spray cloud starts moving over the platform of vessels or offshore structures to reach the cold surfaces. The amount of impinging water droplets on the cold surfaces can be predicted by the droplet trajectory method. The duration of the spray cloud is normally shorter than the interval between the spray events. This means marine vessels and offshore structures are repeatedly subjected to a spray cloud for a short period. Ryerson (1995) reported that the average duration of a spray cloud is about 2.7 s. Other studies indicate that the spray duration is typically about 2 s (Borisenkov et al., 1975).

The interval between the spray events can be estimated by assuming spray generation during every fourth wave encounter on a vessel bow (Lozowski et al., 2000). In typical sea conditions

(Zakrzewski, 1987), the average interval between spray events can be estimated as about 60 s. This means that usually in every minute, a spray event of about 2.5 s will occur. For wave-impact sea spray, the spray duration is much shorter than the interval periods. The average time ratio of spray duration and spray intervals is typically about 1/30 (Zakrzewski, 1987).

Intermittent spray clouds move over the superstructures of marine vessels and offshore structures to reach the cold surfaces and substrates (Dehghani et al., 2016a; Lozowski et al., 2000; Zakrzewski, 1987). The water starts freezing after impinging on the cold surfaces. The freezing process is dependent on the atmospheric conditions and the characteristics of the vessels or offshore structures. The variables of wave-spray ice accretion are dependent on time. The process is almost cyclic and repeats several times. Fig. 2 shows the cycle stages of wave-spray ice accretion. This type of ice accretion is different from wind spray ice accretion and atmospheric ice accretion which are almost continuous and steady ice accretion processes.

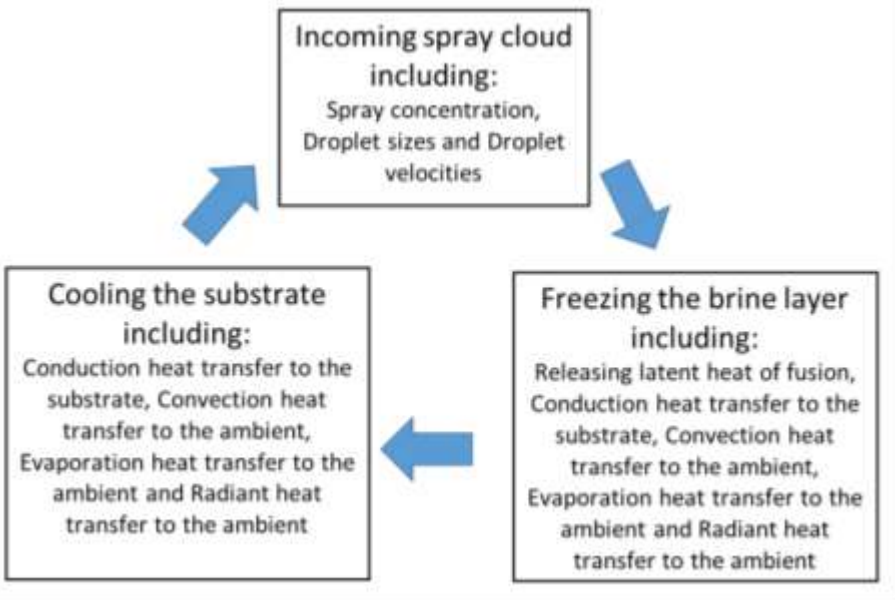

Fig. 2. Main stages of a periodic process of ice accretion.

Incoming spray clouds start the cyclic process by carrying droplets towards cold substrates. Droplets impinge on cold substrates and the freezing process starts. A thin layer of brine is formed on the cold substrates, freezing starts at the phase interface and the latent heat of fusion is released. Heat transfer mechanisms dissipate the released latent heat to the ambient air and substrate. Convection, radiation and evaporation heat transfers cause heat flow towards the ambient air and heat conduction causes transferring the heat towards the cold substrate. After a short time, the brine layer freezes and the new layer of solid ice will be directly in contact with the ambient air. Convection, radiation and evaporation heat transfers start cooling down the substrate. The substrate will be cold enough to be ready for the start of a new cycle. Wave-spray characteristics affect transient ice accretion processes and will be explained in the following sections.

The intermittent ice accretion phenomenon can be divided into two individual processes: cooling and freezing. Because of the short period of spray events, it can be concluded that for a long period, the front surface of the substrate will be dry and the surface will become colder due to heat transfer to the environment and sublayers of ice. In this paper, this stage is called the *cooling stage*. In the *freezing stage*, the outer surface of ice is wet with a thin layer of unfrozen brine. A new ice layer, which is confined by the old substrate and the brine layer, exists at this stage. Fig. 3 illustrates the freezing and cooling stages.

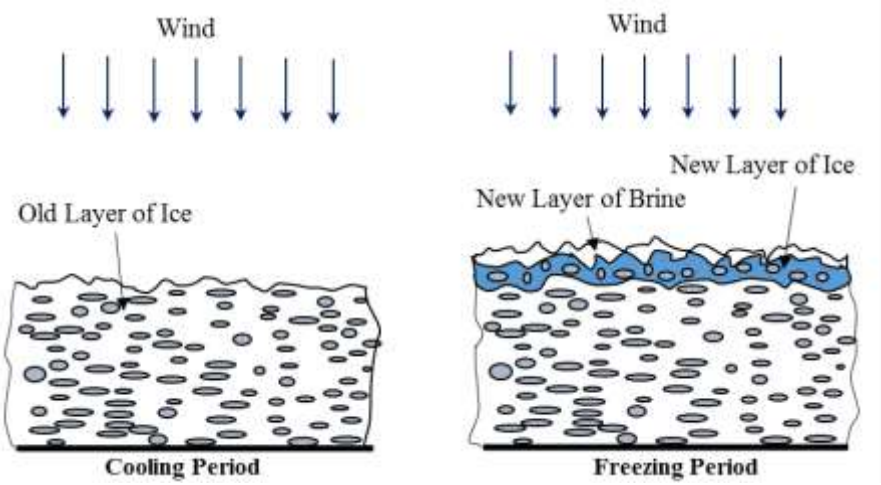

Fig. 3. Illustration of the freezing and cooling stages.

Latent heat released from the phase interface is dissipated during the ice accretion (Shakeel, 1987; Weeks, 2010; Weeks and Ackley, 1986). During the freezing process, heat conduction, convection, radiation, heat transfer due to evaporation and heat released due to solidification are relevant heat transfer processes (Kulyakhtin and Tsarau, 2014; Lozowski et al., 2000). The control volume around the phase interface includes a thin layer of brine (Horjen, 2015; Kulyakhtin and Tsarau, 2014; Lozowski et al., 2000; Shipilova et al., 2012).

In the freezing stage, the heat balance is affected by heat conduction through the substrate of ice, heat convection to the ambient air, radiation to the surroundings, heat transfer due to evaporation of the brine layer, heat transfer due to the incoming supercool droplets and heat released due to the solidification of the brine. It is assumed that the temperature of the brine layer is constant and equal to the freezing point (Horjen, 2015; Kulyakhtin and Tsarau, 2014; Lozowski et al., 2000). Previous studies neglected heat conduction through the substrate of ice. They considered the other heat flows to be the main contributors in the heat balance (Horjen, 2015; Kulyakhtin and Tsarau, 2014; Lozowski et al., 2000; Shipilova et al., 2012). Fig. 4 illustrates the important factors of the heat transfer in the freezing stage.

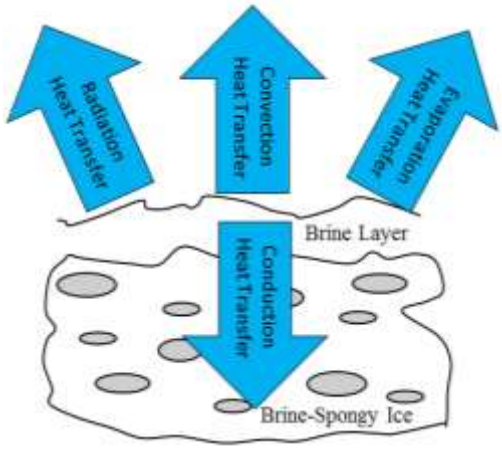

Fig. 4. Heat transfer factors in the freezing stage.

In the process of the cooling the outer surface of the substrate of ice, heat transfer factors are heat conduction through the substrate, convection and evaporation to the ambient air and radiation to the surroundings. Heat flow through the brine-spongy substrate affects the brine pockets and the confined pure ice. Cooling will solidify a portion of brine pockets to pure ice and heat flow will also melt a portion of pure ice and join it to the brine pockets (Weeks and Ackley, 1986). This implies that the cooling and heating cause an exchange of sensible heat and latent heat energy in the brine-spongy ice. Fig. 5 shows the heat flows in the cooling stage.

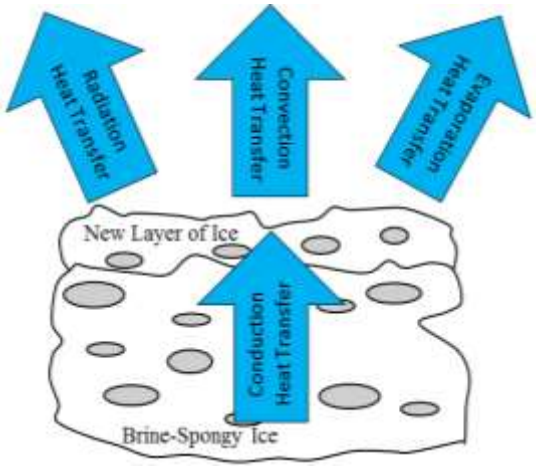

Fig. 5. Heat transfer factors in the cooling stage.

3. Formulation and Modelling

3.1 Heat transfer

Models for calculating convective heat transfer for cylinders and planar components were presented previously (Horjen, 2015; Kulyakhtin and Tsarau, 2014; Lozowski et al., 2000; Shipilova et al., 2012). Important variables in these relations are the relative velocity of air and objects, air temperature and the length scales. Evaporative heat transfer, which is caused by evaporation of brine, represents another significant variable in the solidification. The factors of relative humidity and ambient pressure are needed to calculate the evaporative heat transfer. Convection heat flux is calculated using the relevant formula used by previous researchers (Kulyakhtin and Tsarau, 2014; Lozowski et al., 2000):

$$Q_h = h(T_b - T_a) \tag{1}$$

The convection heat transfer coefficient is calculated using:

$$h = \frac{Nuk_a}{L} \tag{2}$$

Nusselt numbers for cylindrical and planar components are respectively equal to (Szilder and Lozowski, 2000):

$$Nu = 3.0Re^{0.5} \tag{3}$$
$$Nu = 0.036Pr^{0.33}Re^{0.8} \tag{4}$$

Reynolds number of the component is defined as follows:

$$Re = \frac{\rho_a U_r L}{\mu_a} \tag{5}$$

Evaporation heat flux is calculated using the following equation (Kulyakhtin and Tsarau, 2014; Lozowski et al., 2000):

$$Q_e = h\left(\frac{Pr}{Sc}\right)^{0.63} \frac{\varepsilon L_{Hv}}{P_a c_a}\left(e_s(T_b) - RHe_s(T_a)\right) \tag{6}$$

Radiant heat flux is calculated using (Lozowski et al., 2000):

$$Q_r = \sigma(\varepsilon_b T_b^4 - \varepsilon_a T_a^4) \tag{7}$$

The contribution of brine pockets in the conductive heat transfer through brine-spongy ice creates a phenomenon that acts like a thermal capacitor. In a transient condition, heat cannot flow

through brine-spongy ice without melting a portion of the ice. Brine-spongy ice cannot become colder without freezing a portion of the brine pockets (Shakeel, 1987; Weeks, 2010; Weeks and Ackley, 1986).

Fig. 6 illustrates varying sizes of brine pockets at the end of the freezing and cooling stages. At the end of the freezing stage, the brine-spongy ice exists at the highest temperature. The brine pockets exist at the maximum volume, and consequently, the volume fraction of brine is at a maximum. This stage is a thermally discharged stage. The cooling stage is a stage of charging the brine spongy ice thermally. By cooling the brine-spongy ice, a portion of brine pockets starts to freeze, and at the end of the cooling stage, the brine pockets exist at the minimum volume. In this stage, the volume fraction of brine is minimal.

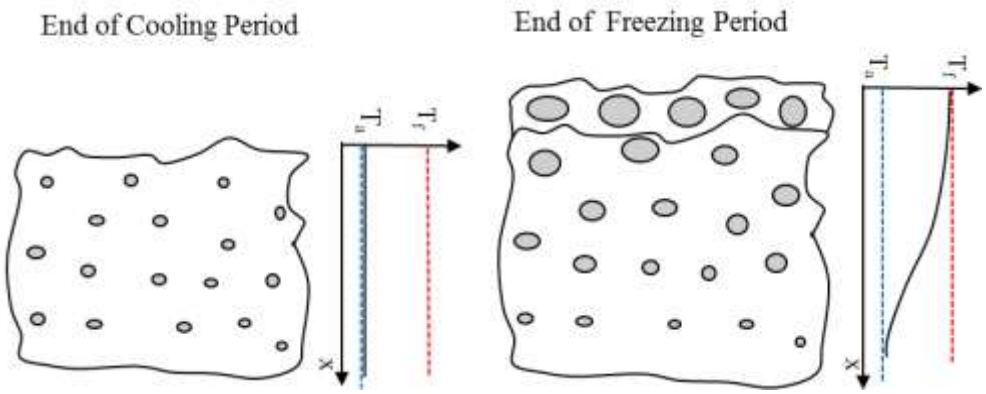

Fig. 6. Illustration of the role of thermal capacitance in brine-spongy ice accretion.

Cooled brine-spongy ice has a significant capacity to absorb heat. Due to the contribution of latent heat, this capacity is enhanced. The process of cooling brine-spongy ice increases its thermal capacity until all of the brine pockets are frozen. The temperature of completely frozen brine pockets is about -21 ^{o}C (Shakeel, 1987; Weeks, 2010; Weeks and Ackley, 1986). This means brine-spongy ice can act as a thermal capacitor in a temperature range from the start of the freezing point to about -21 ^{o}C. At temperatures less than -21 ^{o}C, there are only ice and solid salt phases. At those temperatures, the latent heat mechanism cannot be active; therefore, the brine-spongy ice behaves like a solid material.

3.2 Brine-spongy ice

The governing equation of heat transfer in brine-spongy ice, proposed by Dehghani et al. (2017), is obtained as:

$$\rho_e \, c_e \frac{\partial T}{\partial t} = \vec{\nabla}.\left(k_s \, \vec{\nabla} T\right) \tag{8}$$

$$\rho_e \, c_e = \left(\rho_s \, c_s - \frac{S \, \rho_i \, L_{Hb}}{T^2} 49.185 \times 10^{-3}\right) \tag{9}$$

This partial differential equation is dependent on the overall salinity and thermal properties of brine pockets, ice and brine-spongy ice. Table 1 shows relations which describe the thermal properties of ice, brine and brine-spongy ice (Cox and Weeks, 1975; Weeks, 2010; Weeks and Ackley, 1986).

Eq. (8), Eq. (9) and the equations of properties in Table 1 yield 13 equations and 13 unknowns leading to a set of linear and nonlinear equations. The unknowns are temperature, brine conductivity, brine heat capacity, brine salinity, brine density, brine heat of fusion, ice density, ice thermal conductivity, ice heat capacity, spongy ice conductivity, spongy ice density, spongy ice heat capacity and volume fraction of brine. Properties of spongy ice are considered as weighted properties of ice and brine. The properties in Table 1 are empirical relations found by previous investigators (Cox and Weeks, 1975; Weeks, 2010; Weeks and Ackley, 1986). These are dependent on the coefficients which are obtained experimentally. Table 2 includes the coefficients in the equations of Table 1. With initial conditions, which are the initial distribution of temperature in the brine-spongy ice, the boundary conditions, and also the overall salinity of brine-spongy ice, this set of 13 equations and 13 unknowns can be solved. The results predict the thermal response of brine-spongy ice at each moment of time.

Table 1. Properties of pure ice, brine, and brine-spongy ice.

Properties	Equations
c_b	$\alpha_{cb0} + \alpha_{cb1}\,T + \alpha_{cb2}\,T^2 + \alpha_{cb3}\,T^3$
c_i	$\alpha_{ci0} + \alpha_{ci1}\,T$
c_s	$c_b \frac{\rho_b}{\rho_s}\,V_{Fb} + c_i(1 - \frac{\rho_b}{\rho_s}V_{Fb})$
k_b	$\alpha_{kb0} + \alpha_{kb1}\,T + \alpha_{kb2}\,T^2$
k_i	$\alpha_{ki0} + \alpha_{ki1}\,T$
k_s	$k_b\,V_{Fb} + k_i\,(1 - V_{Fb})$
L_{Hb}	$\alpha_{LHb0} + \alpha_{LHb1}\,T + \alpha_{LHb2}\,T^2$
S_b	$\alpha_{sb1}\,T + \alpha_{sb2}\,T^2 + \alpha_{sb3}\,T^3$
ρ_b	$\alpha_{\rho b0} + \alpha_{\rho b1}\,S_b$
ρ_i	$\alpha_{\rho i0} + \alpha_{\rho i1}\,T$
ρ_s	$\rho_b\,V_{Fb} + \rho_i\,(1 - V_{Fb})$

Table 2. Coefficients for the equations of the properties in Table 1.

Coefficients	Values			
	(0)	(1)	(2)	(3)
$\alpha_{cb()}$	4211.249	111.437	5.125	93.545×10^{-3}
$\alpha_{ci()}$	2118.5199	7.8000	0	0
$\alpha_{kb()}$	0.5664	3.0822×10^{-3}	1.8388×10^{-5}	0
$\alpha_{ki()}$	2.2399	-10.7517×10^{-3}	0	0
$\alpha_{LHb()}$	-333400.326	-4958.217	-29.894	0
$\alpha_{sb()}$	0	-17.5730	-0.381246	-3.28366×10^{-3}
$\alpha_{\rho b()}$	1000	0.8	0	0
$\alpha_{\rho i()}$	917	-0.1403	0	0

3.3 Wave-impact sea spray

The movement and frequency of spray clouds determine the rate of water delivery to the cold surfaces of the vessel. The extent of the spray is calculated using the formula suggested by Lozowski et al. (2000). In this formula, the maximum travel distance of the spray cloud is calculated by:

$$X_e = 2H_s + 0.04(1.56P + V_s)^2 - 10 \quad (10)$$

Where X_e is the extent of the spray cloud, H_s is the significant wave height, P is the period of the sea wave and V_s is the vessel speed. It is assume that one wave among 3 to 5 waves that strike the vessel can successfully generate a spray cloud.

4. Case Definition and Assumptions

Three categories of information are required to define the case completely for numerical simulations. The first category is related to the sea information including significant wave heights, sea surface temperature, wave period, wave direction and seawater salinity. The second category is the weather condition including wind speed, wind direction, air temperature, relative humidity of air and precipitation. The third category of information is the vessel information including vessel geometry, vessel speed and vessel direction. The data mentioned above are provided by the US National Transportation Safety Board (NTSB).

The model is defined considering two individual conditions, full load and low load conditions. Figs. 7 and 8 show the full and low load conditions. In the full load condition, the vessel is occupied by crab cages. For the low load condition, it is assumed that the necessary equipment is on the deck and there are no cages on the deck. The geometry of the vessel extracted from Figs. 8 and 9. The path of the vessel is shown in Fig. 10.

Fig. 6. A picture of the full load condition

Fig. 7. A picture of the low load condition

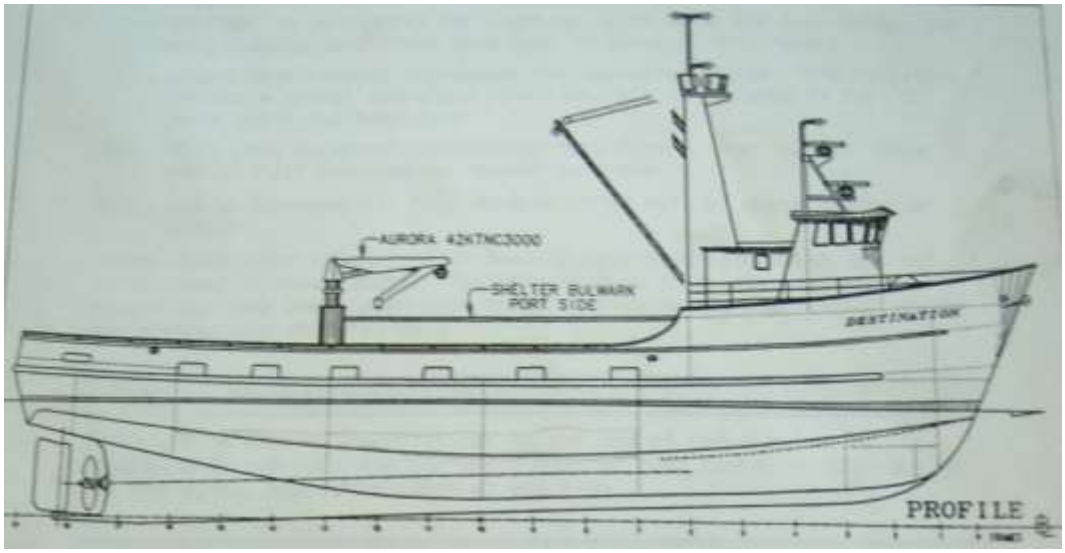

Fig. 8. Side view of the vessel

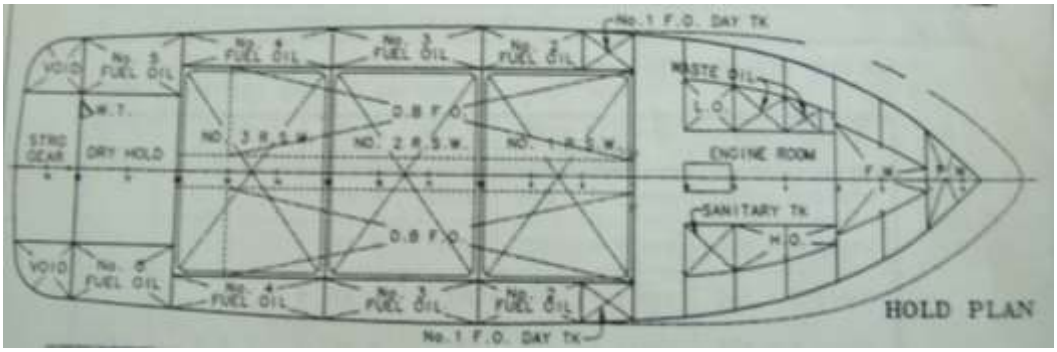

Fig. 9. Top view of the vessel

Fig. 10. The path of the vessel

The significant wave heights and wave period from February 09 to February 11 are shown in Fig. 11. The information of the vessel speed and wind speed can be found in Fig. 12. The air temperature is plotted in Fig. 13.

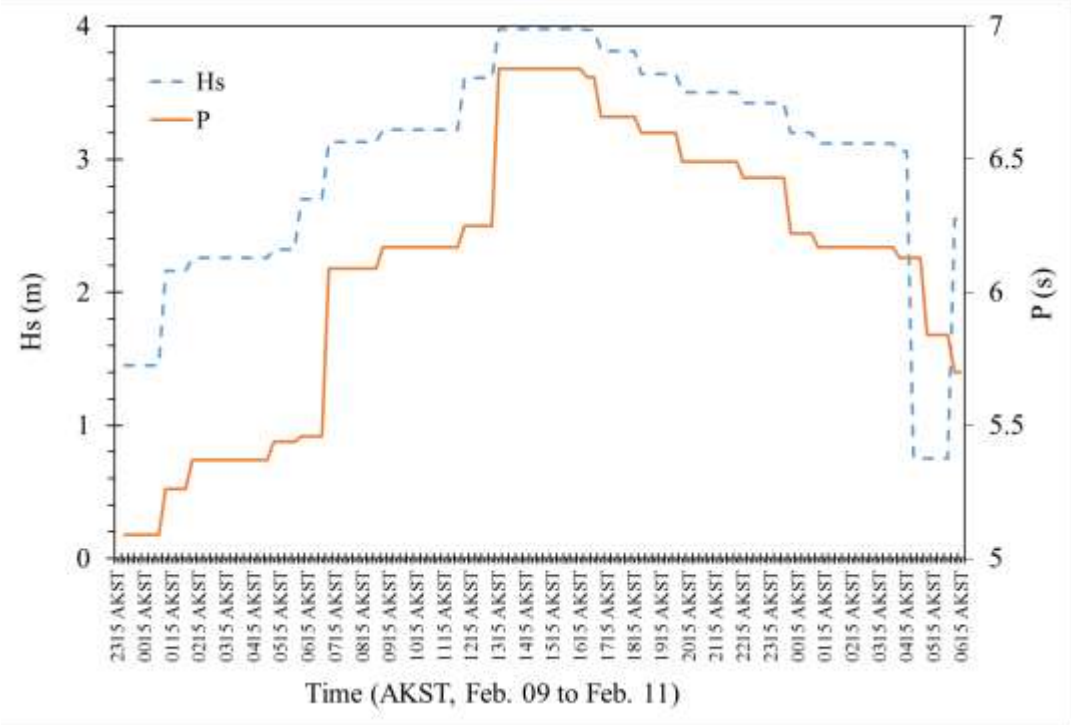

Fig. 11. The significant wave height and wave period during the vessel's travel

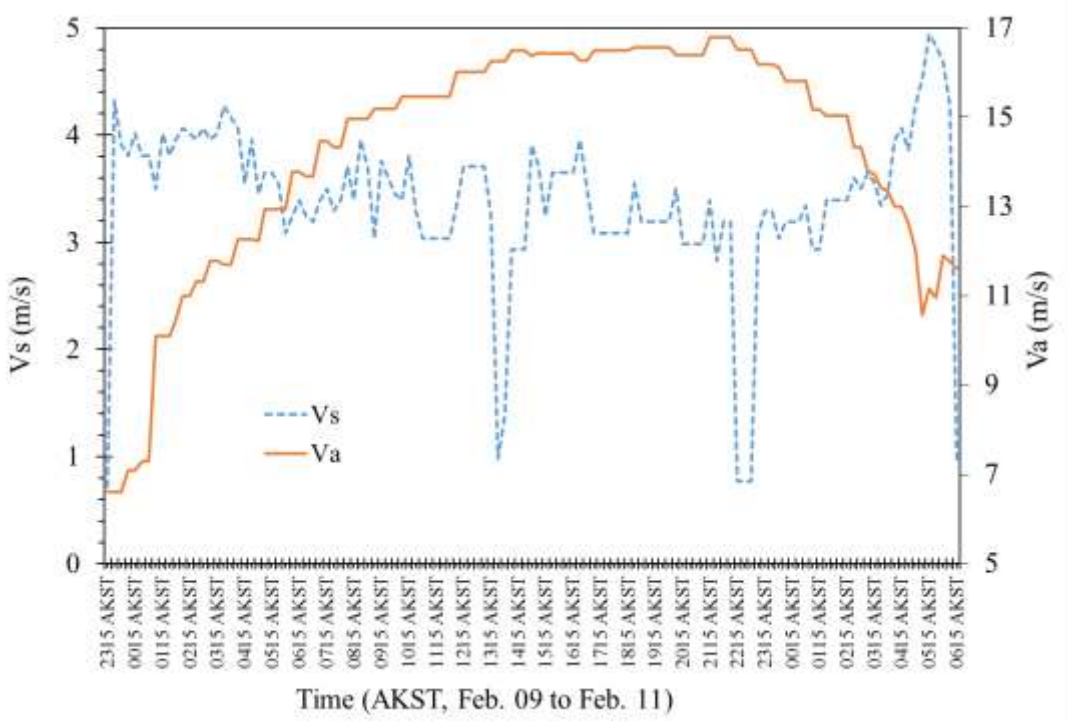

Fig. 12. Vessel speed and wind speed

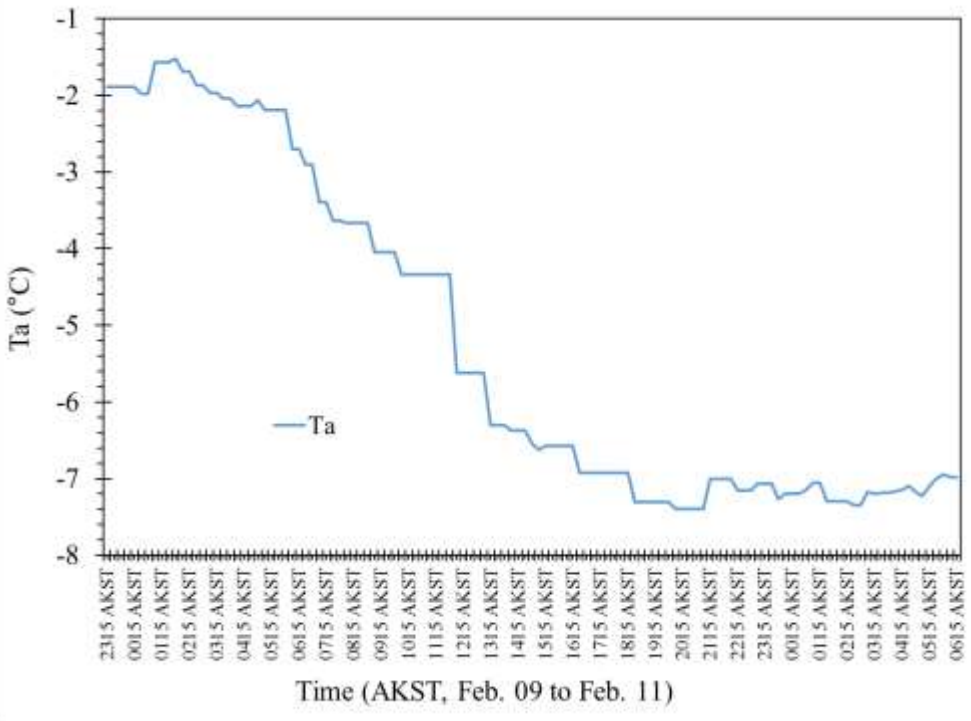

Fig. 13. Air temperature

5. Numerical method

The discretization of the differential equations for the solid and liquid phases for the numerical solution is based on a uniformly-spaced fixed-grid method. The freezing fraction, which is the ratio of the frozen portion of a grid to the total length of the grid, is defined by δ. The right-hand side of the domain represents the brine layer and the left-hand side is the brine-spongy ice. Fig. 14 illustrates the nodes and grid points from $i = 1$ to $i = n + 1$. The phase interface is between $i = m$ and $i = m + 1$. The variable δ, which varies between zero and one, defines the freezing fraction in the solidification grid located between $i = m$ and $i = m + 1$. In order to prevent instabilities when the phase interface is very close to the nodes, $\delta \cong 1$ or $\delta \cong 0$, four interpolated temperatures are introduced: T_{s1}, T_{s2}, T_{b1} and T_{b2}. These temperatures provide a smooth variation of the values of the discretized equations when the phase interface passes a node. For this purpose, it is assumed that temperature varies linearly over the length between two adjacent nodes and the interpolated temperatures are calculated based on their distances to the nodes.

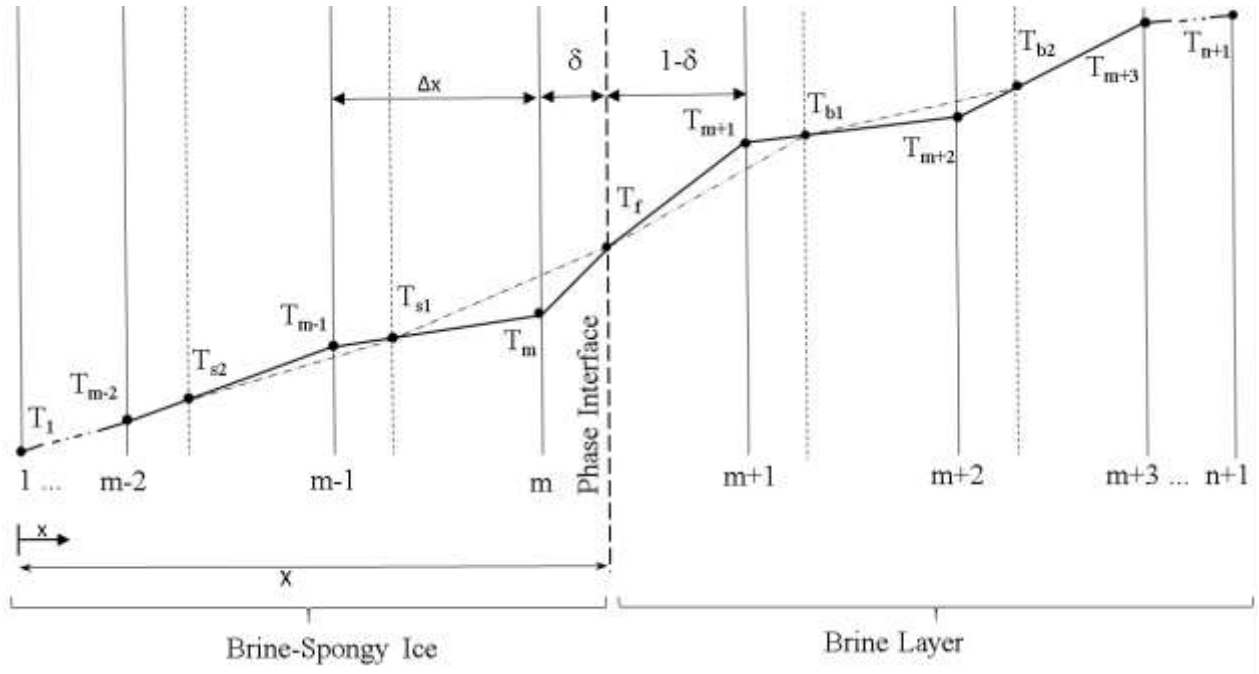

Fig. 14. Discretization of the domain including the brine-spongy substrate and brine layer

A challenging aspect is discretizing the equations at $i = m$ and $i = m + 1$, which are affected by the moving phase interface. As mentioned, the interpolated temperatures are used as the reference temperatures for discretization at $i = m$ and $i = m + 1$. The freezing fraction and the interpolated temperatures are calculated as follows:

$$\delta = \frac{x}{\Delta x} - (m - 1) \tag{11}$$

$$T_{s1} = (1 - \delta)T_{m-1} + \delta T_m \tag{12}$$

$$T_{s2} = (1-\delta)T_{m-2} + \delta T_{m-1} \quad (13)$$

$$T_{b1} = (1-\delta)T_{m+1} + \delta T_{m+2} \quad (14)$$

$$T_{b2} = (1-\delta)T_{m+2} + \delta T_{m+3} \quad (15)$$

$$\frac{dX}{dt} = \frac{1}{\rho_s(T_f)[1-V_{Fb}(T_f)]L_{Hb}(T_f)}\left\{\frac{k_s(T_f)+k_s(T_{s1})}{2}\frac{T_f-T_{s1}}{\Delta x} - \frac{k_b(T_f)+k_b(T_{b1})}{2}\frac{T_{b1}-T_f}{\Delta x}\right\} \quad (16)$$

It is assumed that the first node, $i = 1$, which represents the left end of the brine-spongy substrate, is kept at a constant temperature. Therefore, the temperature variation at $i = 1$ will be equal to zero:

$$\frac{dT_i}{dt} = 0 \qquad i = 1 \quad (17)$$

Discretization of the partial derivative equations on the interior nodes is obtained as follows:

$$\frac{dT_i}{dt} = \frac{1}{\rho_e c_e(T_i)}\left\{\frac{k_s(T_{i+1})-k_s(T_i)}{\Delta x}\frac{T_{i+1}-T_i}{\Delta x} - k_s(T_i)\frac{T_{i+1}-2T_i+T_{i-1}}{\Delta x^2}\right\} \qquad i = 2,\dots,m-1 \quad (18)$$

$$\frac{dT_i}{dt} = \frac{1}{\rho_e c_e(T_i)}\left\{\frac{k_s(T_f)-k_s(T_{s1})}{\Delta x}\frac{T_f-T_{s1}}{\Delta x} - k_s(T_i)\frac{T_f-2T_{s1}+T_{s2}}{\Delta x^2}\right\} \qquad i = m \quad (19)$$

$$\frac{dT_i}{dt} = \frac{1}{\rho_b(T_i)c_b(T_i)}\left\{\frac{k_b(T_{b1})-k_s(T_f)}{\Delta x}\frac{T_{b1}-T_f}{\Delta x} - k_b(T_i)\frac{T_{b2}-2T_{b1}+T_f}{\Delta x^2}\right\} \qquad i = m+1 \quad (20)$$

$$\frac{dT_i}{dt} = \frac{1}{\rho_b(T_i)c_b(T_i)}\left\{\frac{k_b(T_{i+1})-k_b(T_i)}{\Delta x}\frac{T_{i+1}-T_i}{\Delta x} - k_b(T_i)\frac{T_{i+1}-2T_i+T_{i-1}}{\Delta x^2}\right\} \qquad i = m+2,\dots n \quad (21)$$

The outer surface of the brine layer is assumed to be an insulated boundary. Therefore, the temperature variation will be equal to that of the previous node.

$$\frac{dT_i}{dt} = \frac{dT_n}{dt} \qquad i = n+1 \quad (22)$$

The discretized equations, which are arranged based on the MOL, are solved using an iterative method by using variable time steps to calculate the temperatures in the brine and the brine-spongy ice during the freezing process.

6. Results of icing calculations

The mass of ice accumulated on the fishing vessel from 23:15 AKST on Feb. 9, 2017 to 06:15 AKST on Feb. 11 is shown in Fig. 15. Results vary between Max and Min values corresponding to full load and low load conditions. The rate of ice load is shown in Fig. 16. The highest rate of ice accumulation is 2.7 ton/15min which is for 1700 AKST on February 10.

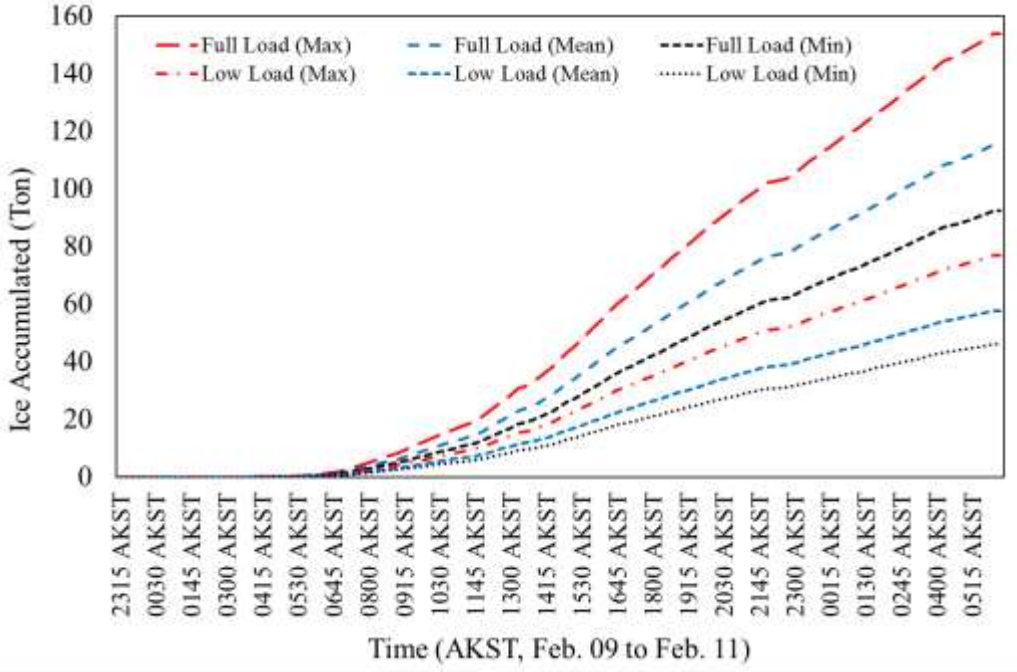

Fig. 15. Numerical solution of the mass of ice accumulated on the fishing vessel (Destination)

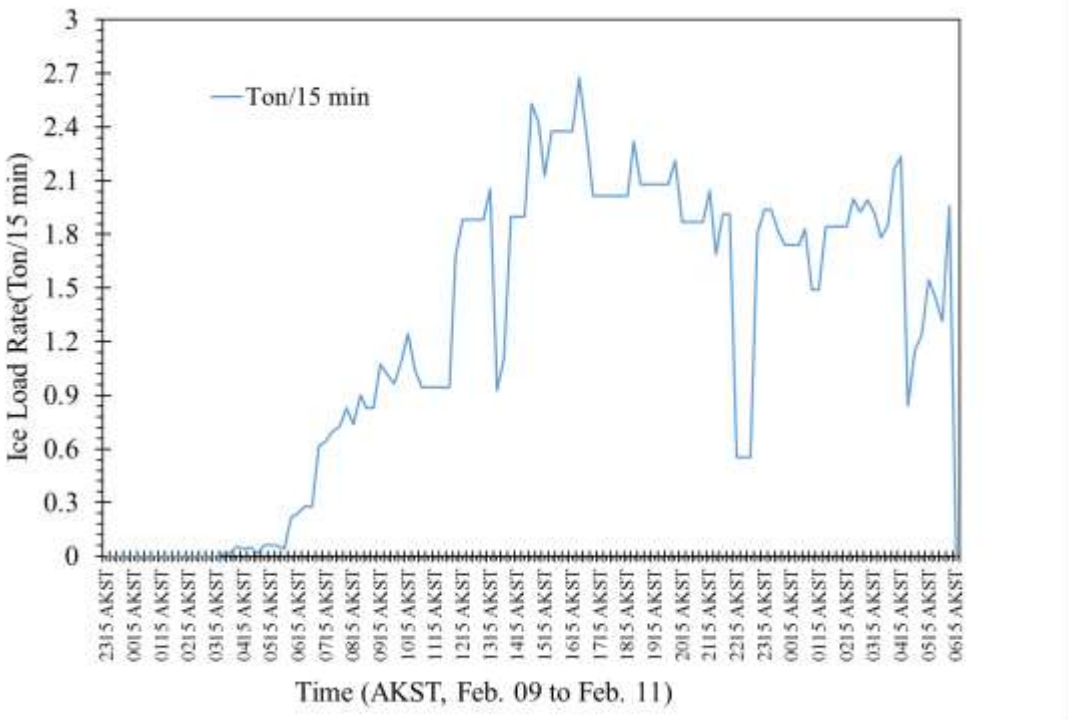

Fig. 16. The rate of ice load accumulated on the vessel

7. Stability Analysis

An approximate analysis of the effect of the predicted icing on the vessel stability was conducted by estimating the loss of metacentric height (GM) associated with a range of ice accumulation values and a range of heights of the effective center of gravity of the accumulated ice. GM is a measure of the small angle static stability of a vessel and is a measure of the difference between the vertical center of gravity (G) of the vessel and the height of the metacenter (M). Metacenter can be thought of as the radius of the shift in center of buoyancy as a vessel inclines and thus the distance GM is effectively a measure of the restoring moment arm for small angles of vessel inclination. This is the most commonly used index of vessel stability and is relatively easy to calculate.

In the present case, the GM of the vessel is unknown and the analysis calculates a change in GM associated with the accumulated ice. The change in GM arises from a shift in G associated with the added weight of the ice and from a smaller shift in M associated with the increase in the hull submerged volume due to the increased displacement associated with the added weight of ice. This approach was taken because the stability and loading condition of the vessel for the departure condition are unknown and thus a precise analysis cannot be conducted. In addition certain hydrostatic or hull form parameters are unknown (although possibly obtainable) so values typical of fishing vessels are used. Obtaining these hull parameters would not materially improve the estimate of GM change.

Fishing vessels typically operate with GM values no lower than 0.35 m and generally not much greater than 1.0m. However fishing vessels take on cargo at sea as part of their operation and are frequently modified, or loaded without stability assessments. These actions rarely result in increasing levels of stability and thus it is not unusual for fishing vessels to operate with GM values below the recommended range. In the present case the GM value for the vessel as it existed at the time of the sinking or at the time of port departure is unknown.

Table 3 gives the values used in making the stability loss estimates and the output values for a single case. Table 4 gives a summary of output values for all the cases that were considered. Figure 17 provides the values of Table 4 in graphical form.

Table 3. Input and output values for a single Stability Loss Case

FV Destination - Stability changes based on Icing Predictions			
Assumed vessel condition			
Vessel initial displacement	650	tonnes	Calculated based on parameters below
	634	m^3	Calculated volume of displacement
Assumed initial GM	1	m	Assumed at 1 to calculate deviations
Estimated KG	4	m	just above main deck (typical value)
Estimated draft	3.11		
Estimated KB	2.07	m	2/3 of draft (typical value)
Estimated Sinkage	235.2	t/m	Calculated based on parameters assumed

Inferred BM	2.93		= GM-KB+KG
Assumed Ice accumulation			
Weight of ice	150	tonnes	From Simulation
Added displacement	146.3	m^3	Calculated based on Sinkage
VCG of Ice (average)	9	m	WRT Keel
Changes in vessel condition arising from ice accumulation			
New Draft	3.75		Extra weight from ice
New KG	4.94		Change in value from ice accumulation
New BM	2.38		Change in value from ice accumulation
New KB	2.39		Change in value from ice accumulation
New GM	-0.17		Change in value from ice accumulation
Reduction in GM	1.17		Estimated loss of Stability from ice accumulation
Basic Vessel Parameters			
LOA (overall length)	33.5	m	Taken from Trim and Stability book excerpt
Beam	9.8	m	Taken from Trim and Stability book excerpt
Hull Depth (to main deck)	3.9	m	Taken from Trim and Stability book excerpt
LBP (length for calculation)	32	m	Estimated based on typical values
Block Coefficient	0.65		Estimated based on typical values
Waterplane coefficient	0.75		Estimated based on typical values

Table 4. Summary of Metacentric height (GM) reductions for all cases considered

Table of GM Reductions (-m)			
Ice VCG (m)	9	7.5	6
Ice (tonnes)	700 tonnes displacement		
150	1.05	0.79	0.52
125	0.91	0.68	0.46
100	0.76	0.57	0.38
75	0.59	0.45	0.30
Ice (tonnes)	650 tonnes displacement		
150	1.17	0.89	0.61
125	1.01	0.77	0.53
100	0.84	0.64	0.44
75	0.66	0.51	0.35

These calculations are estimates based on a range of possible scenarios both in terms of vessel condition and in terms of ice accumulation. Some parameters concerning the hull form might be

better defined but the loading and operating condition for the vessel at the departure or at the time of the loss cannot be known precisely. Since the vessel was known to be heavily loaded at departure, two cases of 700 tonnes and 650 tonnes displacement, before icing, were considered. Conclusions should be considered as estimates of likely outcomes rather than exact calculations.

The results of this analysis are expressed in terms of loss of metacentric height for a range of vessel conditions and ice accumulations. Predicted losses of GM range from, a low of 0.30 m, for 75 tonnes of ice accumulation at 6 m VCG, assuming the vessel displacement at 700 tonnes, to a high of 1.17 m, for 150 tonnes of ice accumulation at 9 m VCG assuming the vessel displacement at 650 tonnes. It appears unlikely that the vessel had an initial GM higher than 0.75m and thus it is likely that any ice accumulation greater than 100 tonnes would have placed the vessel in a stability compromised condition. Accumulations approaching150 tonnes would be enough to result in a complete loss of stability.

In the compromised position the vessel would have been vulnerable to capsizing due to extreme waves in either beam or following seas and in the case of a complete loss of stability capsizing would have been inevitable, regardless of sea state.

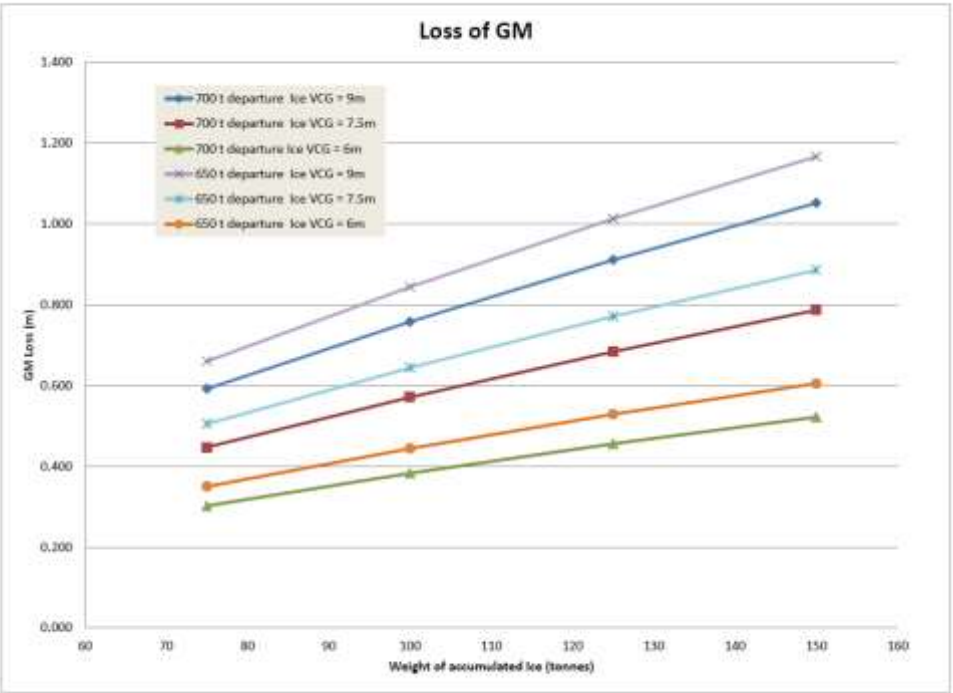

Fig. 17. Loss of Metacentric Height (GM) associated with ice load accumulated on the vessel

8. Conclusion

The method of active cold surfaces is employed to model ice accretion on FV Destination, a fishing vessel that sank in the Bering Sea in February 2017. The data used for this simulation is provided

by NTSB and results are strongly dependent on the input data. The main assumptions for this simulation are the frequency of the spray generation after wave impact, the area of cold surfaces for ice accretion, sufficient sea spray due to harsh weather, transient-rapid freezing of brine and interpolation for the gaps between input data points. The simulation shows that the ice accumulated on the full load vessel would be between 154 ton and 92 tonnes. Assuming an empty vessel the ice load decreases to the range of 77 to 46 ton. The rate of ice accretion before 0600 AKST on February 10 is negligible. The rate of ice accretion increases to the maximum rate in less than 11 hours. The maximum rate of ice accretion occurred at 1700 AKST on February 10, which is about 2.7 ton/15min. It remains high, more than 1.8 ton /15 min, for the rest of the time.

Based on the higher range of ice accumulation estimates, the effect of icing on the vessel stability, as expressed by the measure of metacentric height (GM), was estimated and it is concluded that the predicted ice accumulation would have had sufficient influence to either severely compromise, or completely eliminate, the vessel stability. This would result in a high probability of capsize associated with the predicted levels of ice accumulation.

References

Blackmore, R.Z., Lozowski, E.P., 1994. An Heuristic Freezing Spray Model of Vessel Icing. Int. J. Offshore Polar Eng. 4.

Bodaghkhani, A., Dehghani, S.-R., Muzychka, Y.S., Colbourne, B., 2016. Understanding spray cloud formation by wave impact on marine objects. Cold Reg. Sci. Technol.

Borisenkov, Y.P., Zablockiy, G.A., Makshtas, A.P., Migulin, A.I., Panov, V. V, 1975. On the approximation of the spray cloud dimensions, in: Arkticheskii I Antarkticheskii Nauchno-Issledovatelskii Institut. Gidrometeoizdat Leningrad, pp. 121–126.

Cox, G.F.N., Weeks, W.F., 1975. Brine Drainage and Initial Salt Entrapment in Sodium Chloride Ice., CRREL Research Report. DTIC Document.

Dehghani-Sanij, A.R., Dehghani, S.R., Naterer, G.F., Muzychka, Y.S., 2017. Sea spray icing phenomena on marine vessels and offshore structures: Review and formulation. Ocean Eng. 132, 25–39.

Dehghani, S.R., Muzychka, Y.S., Naterer, G.F., 2018. A finite difference solution for freezing brine on cold substrates of spongy ice. Int. J. Heat Fluid Flow 69, 174–184.

Dehghani, S.R., Muzychka, Y.S., Naterer, G.F., 2016a. Droplet trajectories of wave-impact sea spray on a marine vessel. Cold Reg. Sci. Technol. 127, 1–9. doi:10.1016/j.coldregions.2016.03.010

Dehghani, S.R., Naterer, G.F., Muzychka, Y.S., 2018. 3-D trajectory analysis of wave-impact sea spray over a marine vessel. Cold Reg. Sci. Technol. 146, 72–80. doi:10.1016/j.coldregions.2017.11.016

Dehghani, S.R., Naterer, G.F., Muzychka, Y.S., 2017. Transient heat conduction through a substrate of brine spongy ice. Heat Mass Transf.

Dehghani, S.R., Naterer, G.F., Muzychka, Y.S., 2016b. Droplet size and velocity distributions of wave-impact sea spray over a marine vessel. Cold Reg. Sci. Technol. 132, 60–67. doi:10.1016/j.coldregions.2016.09.013

Forest, T.W., Lozowski, E.P., Gagnon, R., 2005. Estimating Marine Icing on Offshore Structures using RIGICE04. Iwais Xi.

Hay, R.F.M., 1956. Meteorological Aspects of the Loss of the Lorella and Roderigo. Mar. Obs. 26, 89–94.
Horjen, I., 2015. Offshore drilling rig ice accretion modeling including a surficial brine film. Cold Reg. Sci. Technol. 119, 84–110. doi:10.1016/j.coldregions.2015.07.006
Jorgensen, T.S., 1982. Influence of ice accretion on activity in the northern part of the Norwegian continental shelf. Offshore Technology Testing and Research Group.
Kulyakhtin, A., Tsarau, A., 2014. A time-dependent model of marine icing with application of computational fluid dynamics. Cold Reg. Sci. Technol. 104–105, 33–44. doi:10.1016/j.coldregions.2014.05.001
Lozowski, E.P., Szilder, K., Makkonen, L., 2000. Computer simulation of marine ice accretion. Philos. Trans. R. Soc. London A Math. Phys. Eng. Sci. 358, 2811–2845. doi:10.1098/rsta.2000.0687
Paul Zakrzewski, W., Lozowski, E.P., Muggeridge, D., 1988. Estimating the extent of the spraying zone on a sea-going ship. Ocean Eng. 15, 413–429. doi:10.1016/0029-8018(88)90008-X
Ryerson, C.C., 2011. Ice protection of offshore platforms. Cold Reg. Sci. Technol. 65, 97–110. doi:10.1016/j.coldregions.2010.02.006
Ryerson, C.C., 1995. Superstructure spray and ice accretion on a large U.S. Coast Guard cutter. Atmos. Res. 36, 321–337. doi:10.1016/0169-8095(94)00045-F
Schiesser, W.E., Griffiths, G.W., 2009. A Compendium of Partial Differential Equation Models : Method of Lines Analysis with Matlab, Simulation. doi:10.1017/CBO9780511576270
Shakeel, T., 1987. Dynamics of spontaneous pattern formation in dendritic ice crystal growth.
Shekhtman, A.N., 1971. The Probability and Intensity of the Icing-Up of Ocean-Going Vessels. DTIC Document.
Shipilova, O., Kulyakhtin, A., Tsarau, A., Libby, B., Moslet, P.O., Løset, S., 2012. Mechanism and dynamics of marine ice accretion on vessel archetypes. Soc. Pet. Eng. - Arct. Technol. Conf. 2012 1, 491–502.
Szilder, K., Lozowski, E.P., 2000. Numerical simulations of pendant ice formations. Cold Reg. Sci. Technol. 31, 1–11. doi:10.1016/S0165-232X(99)00035-X
Weeks, W., 2010. On sea ice. University of Alaska Press.
Weeks, W.F., Ackley, S.F., 1986. The growth, structure, and properties of sea ice, in: The Geophysics of Sea Ice. Springer, pp. 9–164.
Zakrzewski, W.P., 1987. Splashing a ship with collision-generated spray. Cold Reg. Sci. Technol. 14, 65–83.